Al_2O_3-supported Pt/Rh catalysts for NO_x removal under lean conditions

L. Castoldi[1*], R. Matarrese[1], M. Daturi[2], J. Llorca[3], L. Lietti[1*]

[1]*Politecnico di Milano, Laboratory of Catalysis and Catalytic Processes, Dipartimento di Energia, Via La Masa, 34, 20156 Milano (Italy)*

[2]*Normandie Université, ENSICAEN, UNICAEN, CNRS, Laboratoire Catalyse et Spectrochimie, 14000 Caen, France*

[3]*Institute of Energy Technologies and Centre for Research in Nanoengineering, Universitat Politècnica de Catalunya, Barcelona, Spain*

**corresponding author: luca.lietti@polimi.it; lidia.castoldi@polimi.it*

Abstract

In this work the reactivity of Pt-Rh NOx storage-reduction (NSR) catalysts in the reduction of NOx under lean conditions is investigated. It is found that significant amounts of NOx are stored on both Rh- and Pt-based samples at all the investigated temperatures (in the range 150–350¿°C). Mostly chelating nitrites are adsorbed at the lowest investigated temperature (150¿°C), while nitrates (both bidentate and ionic) at higher temperatures. However, at all temperatures nitrites prevail at the beginning of the storage phase, while nitrates represent the most abundant adsorbed species after prolonged contact. Pt-containing catalysts (either monometallic Pt or bimetallic Pt/Rh) show higher NOx storage capacity than the Rh monometallic sample, possibly due to the higher dispersion of Pt vs. Rh and/or to the higher oxidizing capability of Pt vs. Rh.

The stored NOx species show relevant thermal stability, and decompose to NOx and O2 upon heating. In particular, nitrites disproportionate to gaseous NO and nitrates; these latter then decompose to NOx and O2. On the Rh-Ba/Al2O3 catalyst the disproportionation reaction is observed with a higher temperature onset if compared to the Pt-based samples. The analysis of the reactivity of the stored NOx species (probed by isotopic labeling experiments and reduction with H2 and NH3) showed the lower reactivity of the Rh-Ba/Al2O3 sample; however Rh shows activity in the ammonia decomposition reaction to N2 and H2, unlike Pt. The lower reactivity of the Rh-Ba/Al2O3 sample is also pointed out by experiments under cyclic lean-rich conditions. However, the presence of Rh increases the reactivity of the catalyst in the steam reforming of hydrocarbons, especially at high temperature, and accordingly the reactivity of the bimetallic Pt/Rh sample at high temperatures is higher than that of the Pt and Rh monometallic catalysts.

1. Introduction

The push for better fuel economy and lower vehicular CO_2 emissions has led to increased deployment of lean-burn engines, being widely used in heavy duty diesel and light duty gasoline engine. However, exhaust gases from these engines contain NO_x and excess O_2, which renders NO_x reduction into N_2 impractical over conventional three-way catalysts (TWCs) [1]. Consequently, two main technologies have been developed for mobile lean NO_x removal, i.e. selective catalytic reduction (SCR) of NO_x using urea as a reductant for heavy duty diesel applications [2,3], and lean NO_x trap (LNT) catalysts (otherwise known as NO_x adsorber or NO_x storage-reduction catalysts) for light duty applications [4]. NSR operation is cyclic: during the lean phase, NO_x is trapped on the catalyst; intermittent rich excursions are used to reduce the NO_x to N_2 and restore the original catalyst surface, after which lean operation resumes [5]. Platinum and barium deposited on γ-Al_2O_3 (Pt-Ba/Al_2O_3 catalyst) is the most commonly studied model composition for NO_x storage-reduction catalysis. Unfortunately, this catalytic system exhibits good catalytic performance at temperatures higher than 300°C; consequently, the low temperature activity of LNT catalysts becomes important, being for light duty

diesel applications typical engine-out temperatures in the EOC (Efficiency Optimization Control) and FTP-75 (Regulatory Vehicle Mode) about 180-350°C [6]. Therefore, the low-temperature performance of LNT catalysts is becoming increasingly important in order to facilitate the implementation of highly fuel efficient lean-burn engines.

A number of efforts have been made to improve the low temperature activity of LNT catalysts; between them, different dopant species have been considered in the catalyst formulation, for example Mn, Fe [7], or Ce [8]. Kim et al. studied the effect of Co and Rh promoter [9]. From these studies, it is evident that doping Pt-Ba/Al catalysts with redox active metal oxides can improve their NO_x storage capacity at low temperature.

In this work, we have considered the effect of Rh promoter in the classical Pt-Ba/alumina formulation focusing the attention of the fundamental aspects of the reactions occurring during the typical lean-rich cycling of the catalyst. Pt-Rh-Ba/Al_2O_3 bimetallic catalyst, and the monometallic reference ones, has been prepared and deeply characterized by means of BET, XRD, XPS and TEM analysis. FT-IR has been used to characterized the nature of the stored NO_x species, while TPD and TPIE for the thermal stability and the reactivity. Finally, isothermal lean-rich cycles using a complex reducing mixture (i.e. H_2 + CO + C_3H_6) have been useful for the reactivity in the NO_x removal and selectivity of this process.

2. Materials and Methods

Model Pt-Rh-BaO/Al_2O_3 (1/0.5/20/100 w/w/w) bimetallic sample has been prepared by incipient wetness impregnation of a commercial γ-alumina (Versal 250 UOP) support with $Pt(NO_2)_2(NH_3)_2$ (Strem Chemicals, 5% w/w) aqueous solutions at first, and $Rh(NO_3)_3$ (Sigma Aldrich, 10% w/w) solution later on, followed by impregnation with $Ba(CH_3COO)_2$ (Sigma Aldrich, 99% w/w) aqueous solution. After each impregnation step the samples have been dried at 80°C overnight and calcined at 500°C for 5 h.

Model Pt-BaO/Al_2O_3 (1/20/100 w/w/w) and Rh-BaO/Al_2O_3 (0.5/20/100 w/w/w) monometallic catalysts have been prepared in the same way.

The obtained catalysts have been characterized by BET analysis for specific surface area and pore size distribution by N_2 adsorption–desorption at 77 K (BET method, Micromeritics TriStar 3000 Instrument).

The metal dispersion has been measured by H_2 chemisorption at 40°C over a pre-reduced catalyst with a TPD/R/O ThermoFisher Instrument.

X-ray powder diffraction (XRD) analysis has been performed with a Bruker D8 instrument using graphite monochromated CuKα radiation; the diffraction patterns were collected in the 2θ range of 10 - 70° with a step of 0.05° and a counting time of 12.5 s per step.

High resolution transmission electron microscopy (HRTEM) was carried out using a JEOL 2010F electron microscope equipped with a field emission source at an accelerating voltage of 200 kV. Samples were deposited on holey Cu grids. The point-to-point resolution achieved was 0.19 nm and the resolution between lines was 0.14 nm.

X-ray photoelectron spectroscopy (XPS) was performed on a SPECS system equipped with an Al anode XR50 source operating at 150 mW and a Phoibos MCD-9 detector. The pass energy of the hemispherical analyzer was set at 25 eV and the energy step was set at 0.1 eV. The pressure in the analysis chamber was kept below 10−7 Pa. The area analysed was about 2 mm × 2 mm. Data processing was performed with the CasaXPS program (Casa Software Ltd., UK).

The interaction of NO/O_2 with the catalytic surface has been investigated by IR spectroscopy and temperature-programmed desorption.

NO/O_2 mixture (1000 ppm NO + 3% O_2 in He) has been fed to the IR reactor for the analysis of the surface species. It consists in a “Sandwich” IR cell containing the catalyst (15 mg) in form of self-supported wafer; the gases leaving the cell were analyzed by mass spectrometer (ThermoStar TM GSD 301) and chemiluminescence analyzer (42i-HL MEGATEC). Total flow was 25 cm^3min^{-1} (at 1

atm and 0°C). Surface FT-IR spectra have been collected with a FT-IR Nicolet Nexus spectrometer with 4 cm^{-1} spectral resolution and accumulation of 64 scans using DTGS detector.

The thermal stability/reactivity of the stored species has been characterized by Temperature Programmed Desorption (TPD, up to 400°C @ 10°C/min in He) and by isotopic labelling experiments with ^{15}NO (Temperature Programmed Isotopic Exchange, TPIE). Further details on the experimental procedure and setup can be found elsewhere [10].

The reactivity of the prepared catalysts in the NO_x removal has been studied by means of lean-rich cycles at different temperature in the 150-350°C range. During the 15 min of the lean phase NO / O_2 mixture (1000 ppm NO+ 3% v/v O_2) has been fed to the reactor in a stepwise way; in the subsequent 15 min rich phase the reductant mixture, constituted by H_2 (500 ppm) + CO (1500 ppm) + C_3H_6 (450 ppm), has been fed. During all the experiments CO_2 (1000 ppm) and H_2O (2.5% v/v) are present in the flow. Prior to any catalytic run the catalysts have been conditioned through NO_x lean-rich cycles (typically 3-4 cycles) at 350°C starting from NO/O_2 and H_2 mixtures.

Notably, due to the low reductant concentration, experiments have been carried out under nearly isothermal conditions, i.e. in the absence of significant temperature effects during the experiments.

3. Results and discussion

3.1 Morphological and structural characterization

BET analysis – The composition of the prepared catalysts, the specific surface area, pore volume and pore sizes are reported in Table 1, along with the metal dispersion. Pt-Ba/Al_2O_3 catalyst shows a specific surface area of 140 $m^2 g^{-1}$ with a final metal dispersion near 60 %; Rh-Ba/Al_2O_3 exhibits a specific surface area of 150 m^2g^{-1} with a Rh dispersion near 7 %. The bimetallic system shows the same morphological characteristics as the monometallic ones; it was not possible to measure the metal dispersion.

XRD analysis – In Figure 1 are reported the XRD spectra of the calcined samples. From the XRD patterns it is possible to recognize the characteristic peaks of microcrystalline face-centered cubic γ-

Al_2O_3 (JCPDS 10-425), $BaCO_3$ both monoclinic and whiterite (JCPDS 78-2057 and 5-378, respectively) in all the catalysts. In the samples containing Pt, also the face-centered cubic metallic Pt (JCPDS 4-802) phase was recognized while in the Rh-containing samples, the Rh phase is not identified. It is worth t note that when the Pt is present, Ba is present mainly in the whiterite form, while in the Rh-Ba catalyst also the monoclinic form is detected.

HRTEM analysis – Figures 2A-C show nice images recorded by STEM-HAADF on Pt-Rh-Ba/Al_2O_3 catalyst. This sample exhibits an excellent dispersion of noble metal nanoparticles. The bright spots correspond to the noble metal nanoparticles, which are not agglomerated; they are finely dispersed over the alumina support. The mean particle size of the noble metal nanoparticles is about 2-3 nm. A HRTEM image is shown in Figure 2D. Again in HRTEM mode is hard to distinguish the noble metal nanoparticles, although in some cases it is possible to infer their presence. Given the small size of the noble metal nanoparticles the EDX spectra does not allow to distinguish between Pt and Rh. Also, it is not possible to get lattice fringe images of the noble metal nanoparticles so no individual characterization is possible. In this regard, it is not possible to discuss if the nanoparticles are monometallic or bimetallic.

High resolution TEM images of Pt-Ba/Al_2O_3 catalyst are reported in Figure 3. Figure 3A and its enlargement in Figure 3B show numerous Pt nanoparticles of similar size and extremely well-dispersed. The mean particle size of Pt is about 1-2 nm, indicating a certainly remarkable dispersion of the Pt nanoparticles. In Figure 3C, the EDX spectra recorded in the areas labeled “a” and “b” are shown. Note that Cu signal comes from the TEM grid. The EDX spectrum of area “a does not contain any bright spot corresponding to Pt and shows the presence of Al and O, the last coming from the alumina support as well as Ba; this demonstrates that Ba is distributed all over the alumina support. The EDX spectrum of area “b”, in which it is possible to recognize several bright spot corresponding to Pt nanoparticles, shows in addition to Al, O and Ba, signals of Pt as expected. Finally, Figures 3D and 3E show HRTEM images, where the morphology and dimensions of the alumina flakes are seen. Also in this case, no Ba segregated is observed in any part of the sample.

STEM-HAADF images of Rh-Ba/Al_2O_3 catalyst are displayed in Figures 4A-E. Both individual Rh nanoparticles as well as Rh aggregated nanoparticles are observed. Moreover, comparing with the TEM images of the binary Rh/Al_2O_3 catalyst (not shown), the presence of Ba does not seem to improve dispersion of the noble metal nanoparticles. Also, barium is not identified occurring as a separate phase and it is likely dispersed in all the sample. Figure 4F shows a HRTEM image where only the alumina support crystallites are clearly identified.

XPS analysis – The results of the XPS analysis are reported in Table 2 in terms of surface atomic ratio. First of all, the atomic concentrations of the noble metals and Ba at the surface of the samples determined by XPS are always lower than those of the bulk. The dispersion of Ba is virtually identical in all samples containing this element (2.3-2.4 %).

The dispersion of Rh is also very similar between the different samples containing this element. This could be apparently in contradiction to the TEM results, where the Rh/Al_2O_3 and Rh-Ba/Al_2O_3 samples, for instance, contained agglomerated Rh nanoparticles. However, given their small dimension, the area of the Rh nanoparticles analyzed by XPS includes all the Rh. In other words, it is not possible to distinguish between isolated Rh nanoparticles and agglomerated Rh since everything is indeed analyzed.

3.2 Activity tests

3.2.1 Characterization of the adsorbed species

Effect of temperature – The interaction of NO/O_2 mixture with the surface of Pt-Rh-Ba/Al_2O_3 catalyst has been performed after completely removal of Ba carbonates present over the freshly calcined catalysts and due the weakly adsorbed atmospheric CO_2. After this, the NO/O_2 mixture has been admitted to the IR reactor at different temperatures and the FT-IR spectra are recorded during this phase. Figure 5 shows the results as difference spectra at 150°C, 250°C and 350°C (Figure 5A, B, C, respectively).

The FT-IR spectra recorded during the NO_x storage at 150°C (Figure 5A) show the formation of chelating nitrites on the barium phase with characteristic bands at 1356 and 1233 cm^{-1} related to $\nu_{sym.}(NO_2)$ and $\nu_{asym.}(NO_2)$ modes, respectively. The concentration of such species increases monotonically during storage. In addition, very minor amounts of bidentate nitrates (1565 cm^{-1}, ν(N=O) mode) are formed after long exposure times, by very slow nitrite oxidation, [11;12;13]. By increasing the temperature up to 250°C (Figure 5B), the FT-IR spectra show that at low exposure times mainly nitrites (main band at 1220 cm^{-1}) are formed at the catalyst surface. Nitrites continue to increase with time on stream and, in parallel, both ionic nitrates ($\nu_{asym.}(NO_3)$ mode split at 1403 and 1350 cm^{-1} and $\nu_{sym.}$ (NO_3) mode at 1040 cm^{-1}) and bidentate nitrates at 1546 cm^{-1} start to form. After long exposures the band at 1220 cm^{-1} related to nitrites goes through a maximum and start to decrease in intensity due to the oxidation of nitrites into nitrates. On the other hands, the bands characteristic of ionic nitrates increase markedly. The parallel decrease of the band at 1546 cm^{-1} suggests the transformation of the bidentate nitrates into the ionic ones. The presence of two isosbestic points in the FTIR spectra confirms that both nitrites bidentate nitrates are transformed into ionic nitrates. Finally, the small band near 1755 cm^{-1} might be associated to the formation of N_2O_4 species [14]. Figure 5C shows the FT-IR spectra recorded as a function of time on stream during the NO_x storage at 350°C. In this case, both nitrites and nitrates are almost simultaneously formed. Upon increasing the exposure time, the nitrite species decrease and eventually disappear while the nitrate bands continue to increase. Also in this case the band of bidentate nitrates shows a maximum while those of ionic nitrates grows monotonically with time. At saturation, only nitrates are present on the surface along with minor amounts of N_2O_4 species.

The storage temperature has also a clear effect on the oxidation capacity of the catalyst (i.e. on the amount of NO_2 produced at steady state) and on the NO_x storage capacity. Indeed, at 150°C negligible amount of NO_2 are observed at the end of the lean phase, being near 1.53 10^{-4} mol g_{cat}^{-1} the amounts of NO_x stored mainly as nitrites (see Figure 5A). By increasing the temperature, the concentration of

NO_2 at steady state increases as well, reaching near 200 ppm at 350°C; at the same way increases the storage capacity, resulting 3.89 10^{-4} mol g_{cat}^{-1} at 350°C.

Effect of noble metal – The same characterization of the adsorbed species in the 150-350°C temperature range have been carried out over monometallic Rh-Ba/Al_2O_3 catalyst and the results are reported in Figure 6A, B, C. The results of NOx adsorption for the model Pt-Ba/Al2O3 catalyst are not here reported since they have been already discussed in previous papers of some of us [Lietti et al. ChemCatChem 4 (2012), 55–58; S. Morandi et al. Catalysis Today 231 (2014) 116–124; Castoldi et al. Applied Catalysis B: Environmental 224 (2018) 249–263].

The surface FT-IR analysis performed at 150 °C over Rh-Ba/Al_2O_3 (Figure 6A) shows that, as in the case of Pt-Rh-Ba/Al_2O_3, NO_x adsorption results mainly in the formation of nitrites (bands at 1360 and 1234 cm^{-1}) that grow during storage. In addition, bidentate nitrates (1559 cm^{-1}) are seen after long exposure times. However, at variance to what observed over Pt-Rh-Ba/Al_2O_3, also ionic nitrates (1394 and 1368 cm^{-1}) and monodentate nitrates [15] (band at 1442 cm^{-1}) are likely formed at this temperature. Surface FT-IR analysis recorded at 250°C (Figure 6B) shows the formation of both nitrites and nitrates (i.e. ionic and bidentate nitrates). Of note, differently from the case of Pt-Rh-Ba/Al_2O_3 both nitrites and nitrates increase monotonically with time on stream. As a matter of fact, no transformation of nitrites and bidentate nitrates into ionic nitrates can be observed.

Besides, at 350°C (Figure 6C) the behaviour of Rh-Ba/Al_2O_3 is similar to Pt-Rh-Ba/Al_2O_3: nitrite species are observed only at a very short exposure time which rapidly evolve to ionic and bidentate nitrates. The transformation of bidentate nitrates into the ionic ones is also apparent.

The FTIR experiments performed at low temperature (e.g. 150◦C) over the model Pt-Ba/Al2O3 showed the formation of surface nitrites only. Besides, at higher temperatures (e.g. 250°C) the formation of nitrates (i.e. both ionic and bidentate) was observed, along with nitrites. In particular nitrites were the prevalent species at the initial NOx uptake and their surface concentration showed a maximum with time. Instead, nitrates bands were found to grow monotonically with time and represented the most abundant adsorbed species after prolonged contact. Finally, when the NOx

storage was carried out at 350 °C, nitrites were observed only at the early stages of adsorption while the bands of nitrates markedly increased with time on stream and were the only bands present after long exposure time [Lietti et al. ChemCatChem 4 (2012), 55–58; S. Morandi et al. Catalysis Today 231 (2014) 116–124; Castoldi et al. Applied Catalysis B: Environmental 224 (2018) 249–263].

By comparing the spectra recorded at the end of the lean phase over all the catalytic systems, it clearly appears that at all the investigated temperatures almost the same NO_x surface species are formed. Besides, in all cases and particularly at 150°C higher amounts of NO_x surface species are stored over Pt-Ba/Al_2O_3, being the relative IR bands more intense than in the other cases as already reported [xxx]. Accordingly, the quantitative analysis confirms that Pt-based catalyst stores more NO_x than Rh-one at each temperature (e.g. at 150°C, 3.38 10^{-4} mol g_{cat}^{-1} vs 0.63 10^{-4} mol g_{cat}^{-1}, respectively; at 350°C, 4.89 10^{-4} mol g_{cat}^{-1} vs 1.75 10^{-4} mol g_{cat}^{-1}, respectively). Moreover, Pt-based catalyst exhibits a higher oxidation capacity of NO to NO_2 than Rh-one, mainly at high temperature; indeed, at 350°C the concentration of NO_2 is near 400 ppm over Pt-Ba/Al_2O_3 catalyst and 150 ppm over Rh-Ba/Al_2O_3 catalyst.

The FTIR data collected over the three different catalytic systems indicate that almost the same NOx surface species are formed during the NOx storage. In particular the NO/O2 adsorption at low temperature results exclusively in the formation of nitrites. Besides, upon increasing the temperature the parallel formation of nitrates is observed. Nitrites prevail over the nitrates at the beginning of the storage phase while nitrates represent the most abundant adsorbed species after prolonged contact which indicates that at high temperatures nitrites are intermediates in the formation of nitrates. Of note, the transformation of nitrites into nitrates is slower over Rh-based catalysts. Besides, only in the case of the Rh-containing catalysts the additional transformation of bidentate nitrates into ionic nitrates is observed.

3.2.1 Thermal stability of the stored species

The thermal stability of stored NO_x was evaluated by temperature-programmed desorption (TPD) in flowing He after NO_x adsorption. The NO_x storage process has been carried out at 150ºC, 250°C and 350 ºC where NO_x are stored as nitrites and/or nitrates, according to the spectra already discussed and previous works on Pt-Ba/Al_2O_3 systems [16,17].

TPD profiles obtained after storage at 150°C over the Pt-Rh-Ba/Al_2O_3 catalyst are plotted in Figures 7A. Inspection of Figure shows that the temperature onset for NO_x release is near 125ºC, i.e. slightly lower with respect to the adsorption temperature. Two NO desorption peaks are clearly observed whose maxima are centred at 250ºC and 470ºC. Notably, the high-temperature peak is accompanied by the evolution of O_2.

The TPD profile of the monometallic catalysts are very similar to that of bimetallic one, both as shape as onset temperature. Indeed, as clearly appears from Figure 7B and 7C (i.e. Pt- and Rh-monometallic samples, respectively) a NO desorption peak is observed at low temperature, with a maximum catered near 250°C in the case of Pt-based monometallic system and slightly higher in the case of Rh-based monometallic one. In both cases, a higher desorption peak is observed, being the desorption of NO accompanied in this case by evolution of O_2.

The presence of two desorption steps likely indicates the decomposition of NO_x adsorbed species having different stability. The observation that at low-temperature only NO is released whereas at high temperature the NO evolution is accompanied by O_2 might be explained considering the initial disproportionation of nitrites to nitrate species, as reported and discussed in previous paper [18] and according to reaction (1):

$$3\ Ba(NO_2)_2 \rightarrow Ba(NO_3)_2 + 2\ BaO - 4\ NO\uparrow \qquad (1)$$

Nitrates are then decomposed at high temperatures into NO and O_2, according to reaction (2):

$$Ba(NO_3)_2 \rightarrow BaO + 2\ NO + 3/2\ O_2 \qquad (2)$$

After NO_x adsorption at 350ºC on Pt-Rh-Ba/Al_2O_3 catalyst (Figure 7G), the TPD profile shows a unique decomposition peak, with an onset temperature near 320°C. NO and O_2 evolution is observed, centred near 450ºC. The evolution of small amounts of NO_2 is also observed, with maximum near

420°C. A very similar behaviour is observed when monometallic catalysts are considered (Figure 7H for Pt-catalyst, 7L for Rh-one), being the maximum of NO and O_2 peaks centred always near 320-350°C. It is worth to note the in the presence of Rh the amount of NO_2 detected is lower.

The NO/O_2 ratio evolved during the TPD run is very close to that expected from the decomposition of stored nitrates (reaction (2)). Notably, the NO/O_2 ratio and the peak temperature of the nitrate decomposition closely resembles the high-temperature peak seen during the TPD after NO_x adsorption at 150°C, where nitrites were expected to be formed. This provides additional evidences that the high temperature peak in Figure 7A,7B,7C might be associated to the decomposition of nitrates.

When the NO_x adsorption is performed at intermediate temperature, i.e. at 250ºC (Figure 7D-F), a complex situation is observed; indeed, the TPD profiles resemble the nitrites decomposition (as in Figure 7A-C) or the nitrates decomposition (as in Figure 7G-L), depending on the catalyst formulation. The bimetallic catalyst (Figure 7G) exhibits an important high-temperature peak of NO accompanied by O_2 and a shoulder at lower temperature, i.e. after adsorption at 250°C the TPD profile is intermediate between that of nitrites and that of nitrates suggesting that on the catalyst surface the main species are nitrates while a lower amount of nitrites is still present.

TPD shape of $Pt\text{-}Ba/Al_2O_3$ catalyst after adsorption at 250°C well compares that recorder after adsorption at 350°C (compare Figure 7E and 7H), where FT-IR spectra have shown the presence of only nitrates at catalyst surface. On the other hand, Figure 7F associated with TPD over $Rh\text{-}Ba/Al_2O_3$ catalyst after adsorption at 250°C shows a situation more similar to that reported in Figure 7C after adsorption at 150°C.

TPD experiments clearly demonstrate that by increasing the adsorption temperature form 150°C up to 350°C the population of NO_x stored over the catalyst surface changes from nitrites to nitrates, but this transformation occurs and is almost complete at lower temperature when Pt is present, while in the presence of Rh higher temperatures are required. So, the presence of Pt promotes the oxidation of

nitrites to nitrates but the presence of Rh doesn't permit the complete oxidation due the poor oxidation capacity of Rh metal.

3.2.2 Isotopic exchange experiments between ^{15}NO and stored $^{14}NO_x$ (this part should be better discussed)

Moving from the stability to the reactivity of the stored species, it is important to remember that their reduction involves as a first step the release of NO/NO_2 in the gas phase; these species are eventually reduced to N_2 and other by-products like N_2O and NH_3 over the noble metal components. Moreover, at a molecular level and at the active site-level crucial is the interplay between the gas-phase and the surface analysis during the reaction.

To understand the factors that cause the NO_x release alone and to decouple it from the subsequent reduction to N_2 (or other products) ^{15}NO Temperature Programmed Isotopic Exchange (^{15}NO-TPIE) experiments have been performed over mono- and bimetallic catalysts and the results are reported in Figure 8. In isotopic exchange experiments, [19,20] the stability of unlabeled stored $^{14}NO_x$ has been studied by heating the catalyst in flowing labeled gaseous ^{15}NO (instead of helium as in the TPD). Figure 8A-C and 8D-F show the results of the isotopic exchange both in the case of nitrites and nitrates, respectively.

In all the studied cases, a release of $^{14}NO_x$ is observed simultaneously to a ^{15}NO consumption from the gas phase. Indeed, the first exchange with a corresponding formation of gaseous NO is from about 50-100°C in the case of nitrites and from about 200-250°C in the case of nitrates, and in any cases the temperatures are well below that of thermal desorption (compare with TPD data).

Considering the exchange between nitrites and the gas phase, over Pt-Rh-Ba/Al_2O_3 catalyst (Figure 8A) between 70°C and 250°C consumption of ^{15}NO is observed, accompanied by a correspondent release of ^{14}NO; a high-temperature contribute is observed near 350°C and no NO_2 is detected at any temperature. A very similar situation is observed over the Pt-monometallic system (Figure 8B). Over

Rh-monometallic system, the onset temperature for the isotopic exchange is observed at higher temperature, near 230°C (Figure 8C).

The exchange between labeled ^{15}NO and unlabeled stored nitrites is described by the following reaction:

$$Ba(^{14}NO_2)_2 + 2\ ^{15}NO \rightarrow Ba(^{15}NO_2)_2 + 2\ ^{14}NO\uparrow \quad (3)$$

The results can be explained considering that the stored unlabeled nitrites start to be exchanged already at 50°C and during subsequent heating up to 130–150°C as well, leading to ^{15}NO consumption and ^{14}NO evolution. Above 130–150°C, the partially exchanged stored nitrites decompose according to reaction (1), so that the overall NO_x concentration exceeds the inlet NO concentration value while nitrates are formed. The onset temperature of nitrites decomposition in Figure 8 compares well with that observed during TPD of nitrites in Figure 7, being slightly higher (130–150°C vs. near 125°C) because of the more oxidizing environment. At high temperature, above 250°C, and during the initial part of the hold at 350°C under flow of ^{15}NO in He the so-formed nitrates are exchanged, and a high-temperature contribute is observed. It is worth to note that in the case of Rh-catalyst a shift towards high temperature is observed for both the exchanged NO peak; this shifting is lower when Pt is also present. So, the onset temperature for the isotopic exchange increases in the order: Pt < Pt-Rh < Rh. Moreover, due to the lower oxidizing power of Rh, the high-temperature contribute is lower when Rh is in the catalyst formulation.

When the exchange between unlabeled nitrates and the gas phase is considered, the evolution of ^{14}NO and the consumption of ^{15}NO are observed in all the cases at high temperature, starting from 250°C (Figure 8D-F) and also in this case no NO_2 is detected during the heating ramp.

The exchange between labeled gas phase ^{15}NO and unlabeled stored nitrates is described by the following reaction:

$$Ba(^{14}NO_3)_2 + 2\ ^{15}NO \rightarrow Ba(^{15}NO_3)_2 + 2\ ^{14}NO\uparrow \quad (4)$$

The exchange between NO and stored nitrates is observed from a temperature well below that of thermal decomposition of stored nitrates measured by TPD in He illustrated in the previous paragraph

(i.e., from about 250°C vs. 320°C). The exchange reaction proceeds up to 350°C and during the subsequent hold at this temperature. It is worth to note that in this case occurring the decomposition of nitrates at high temperature, the difference in Pt or Rh-based catalyst is almost negligible. However, in the presence of Rh the extent of exchange is lower than in the presence of Pt. Bimetallic system exhibits an intermediate behavior.

The mechanism for NO isotopic exchange has been already reported in previous work [10] and here resumed for sake of clarity. Upon interaction of unlabeled nitrates species stored at a Ba site with a neighboring metallic site (Pt and/or Rh), unlabeled NO is released in the gas phase and a free BaO site is formed; in the meantime oxygen is left at metal site, leading to oxygen adsorbed on it and/or to oxidized metal site. Since any reductant is present that scavenges the adsorbed oxygen atoms from the metal sites, the process cannot proceed further. Indeed, this is what is seen during the TPD of nitrates where decomposition is observed only at high temperatures, once O-adatoms are released as O_2 in the gas phase.

During TPD of nitrites, where decomposition occurs at lower temperatures than for nitrates, oxygen is scavenged by other nitrites with formation of nitrates. When ^{15}NO is present in the gas phase, adsorbed oxygen atoms are scavenged from Pt sites by ^{15}NO, leading to the formation of labeled nitrites/nitrates adsorbed species. Hence, the exchange occurs between gas-phase ^{15}NO and stored $^{14}NO_x$ and it can be monitored by using labeled molecules as in the case of ^{15}NO-TPIE experiments. In this scheme, metallic Pt centers activate stored nitrites and nitrates that are destabilized and eventually released in the gas phase as NO; for this reason, the NO isotopic exchange could be consider as a redox process. Note that the released NO cannot be further reduced due to the lack of reducing agents.

3.2.3 Reactivity of the stored species towards reducing agent

As already discussed, the NO_x release is a chemical reaction occurring at the Pt/Ba interface and driven by metallic Pt/Rh centers. Therefore, it is expected that the release of stored NO_x is favored in the presence of a reductant, due to the formation of reactive metallic centers.

The reactivity of stored nitrates with different reducing agents (H_2, NH_3) has been previously studied by TPSR experiments [21,22,23]. The study has been enriched here by the reduction of nitrites.

TPSR of nitrates **-** The reactivity of nitrate ad-species stored over bimetallic Pt-Rh-Ba/Al_2O_3 catalysts has been investigated under temperature programming using H_2 or NH_3 as reductant (H_2-TPSR or NH_3-TPSR); the results of the gas phase analysis are reported in Figure 9A and 9B, respectively [24]. When H_2 is employed as reducing agent (Figure 9A), the temperature onset for its consumption is observed near 150°C. At 200°C H_2 is totally consumed and both NH_3 and N_2 are observed as reduction products; neither NO nor N_2O were detected during the reduction. The temperature onset for NH_3 formation is slightly lower than that for N_2, which matches with the temperature of total hydrogen consumption. Initially, H_2 is consumed in the reduction of stored nitrates and only ammonia is formed (reaction (5)). Then, as the reduction front moves along the reactor axis, H_2 is completely consumed and so-formed ammonia becomes reactive in the reduction of stored species (reaction (6)).

$$Ba(NO_3)_2 + 8\ H_2 \rightarrow 2\ NH_3 + BaO + 5\ H_2O \qquad (5)$$

$$3\ Ba(NO_3)_2 + 10\ NH_3 \rightarrow 8\ N_2 + 3\ BaO + 15\ H_2O \qquad (6)$$

The ammonia profile, indeed, shows a minimum in correspondence to the maximum of nitrogen production. Finally, H_2 concentration raises due to the depletion of stored nitrates, nitrogen concentration quickly decays to zero while the ammonia decrease is much slower. At 500°C the hydrogen concentration is very close to the inlet value (2000 ppm).

The data in Figure 9A show that the reduction of stored NO_x is active at temperatures well below that of NO_x thermal decomposition and accordingly the NO_x reduction is a metal-catalyzed process that does not require the thermal release of stored NO_x as the preliminary step [NS LAVORI].

For comparative purposes, Figure 9B-C shows also the results obtained in the case of the H_2-TPSR of nitrates over the Pt- and Rh-monometallic samples, respectively [18,24,25,]. The reduction profile

in the case of Pt-monometallic catalyst (Figure 9B) is very similar to that of bimetallic one, showing i) the consumption of H_2 and formation of ammonia at first; ii) the complete H_2 consumption in correspondence to the consumption of NH_3 and the maximum N_2 production; iii) the increase in H_2 concertation and the decrease in the reduction products. It is notice that the onset of NH_3 and N_2 formation are closer and the H_2 consumption sharper than over the bimetallic system. Over Rh-monometallic system (Figure 9C), only NH_3 is observed between the products with a higher onset with respect to Pt-containing catalysts (200°C vs 170°C). Note that starting from 400°C a small production of N_2 is observed, probably due to the decomposition of ammonia formed by reaction (6). The reactivity of stored nitrates has been studied also using ammonia as reducing agent and the results are reported in Figure 9D-F. Note that in this case isotopically labeled nitrates are present at catalyst surface, being obtained by $^{15}NO/O_2$ adsorption. Over all the catalytic systems the reduction of nitrates by ammonia is slower since the onset of this reaction is observed at higher temperature than the one with hydrogen, and is fully selective to nitrogen, being this the only detected species. As already observed, the Rh-monometallic system results the less active showing the lower amount of reduction products. As already reported [26], the dynamics of the evolution of the three dinitrogen isotopes is the same; the unlabeled $^{14}N_2$ and the single-labeled $^{15}N^{14}N$ species are most abundant, while $^{15}N_2$ accounts for 19% of total N_2 in the Pt-Ba/Al_2O_3 catalyst and lower amount in the other cases.

Finally, over the Rh-containing catalysts, both mono- and bi-metallic catalysts, H_2 is observed between the products starting from 300°C together with an increase in the unlabeled $^{14}N_2$. Since the stored NO_x are isotopically labeled (i.e. $^{15}NO_x$), this species originates only from $^{14}NH_3$; hence, at this temperature the decomposition of ammonia occurs according to reaction (7):

$$2\ ^{14}NH_3 \rightarrow {}^{14}N_2 + 3\ H_2 \qquad (7)$$

TPSR of nitrites **-** The reduction of stored nitrites has been performed both by H_2-TPSR or NH_3-TPSR over all the catalytic systems. In general, with H_2 (Figure 10A-C) occurs at even lower temperatures than nitrates; indeed, in these case H_2 is consumed below 100°C with formation of NH_3

and traces of N_2. Moreover, Pt-containing catalysts are more reactive that Rh-monometallic one, both as onset reduction temperature and reduction extent (i.e. low H_2 consumption and NH_3 formation).

The consumption of H_2 and the NH_3/N_2 production follow the stoichiometry of the global reactions (8) and (9):

$$Ba(NO_2)_2 + 6\ H_2 \rightarrow 2\ NH_3 + BaO + 3\ H_2O \quad (8)$$

$$Ba(NO_2)_2 + 3\ H_2 \rightarrow N_2 + BaO + 3\ H_2O \quad (9)$$

Also in the case of nitrites, when H_2 is used as reductant no NO or N_2O are observed among the products.

In the case of the NH_3-TPSR experiment (Figure 11D-F), the desorption of ammonia is observed at first; indeed, ammonia is being stored on the catalyst upon admission at the beginning of the experiment (not shown in the Figures). From nearly 120°C when Pt is present (and slightly higher temperature in the Rh-monometallic catalyst), a net consumption of ammonia is seen together with the formation of N_2O and N_2 due to the reaction of NH_3 with stored labeled nitrites [27,28]. Nitrogen is by far the most abundant product, with different isotopic composition. The single-labeled isotope (i.e., $^{15}N^{14}N$) is initially observed in greater amounts, whereas the unlabeled ($^{14}N_2$) and double-labeled ($^{15}N_2$) species are seen simultaneously and with a short delay respect to the single-labeled nitrogen reported [26]. The evolution of very small amounts of single-labeled nitrous oxide ($^{15}N^{14}NO$), whose concentration is multiplied by a factor of 10, is also observed at the onset of the reaction, near 100°C in the Pt-containing catalysts and near 180°C on Rh-monometallic sample.

The consumption of NH_3 and the N_2 (and N_2O) production agree with the stoichiometry of the global reaction (10):

$$Ba(NO_2)_2 + 2\ NH_3 \rightarrow 2\ N_2 + BaO + 3\ H_2O \quad (10)$$

These data clearly indicate that ammonia is an effective reductant for the stored NO_x, even the reduction by ammonia is slower than with H_2 being the onset of this reaction observed at higher temperature. As in the case of nitrates, at high temperature over Rh-containing catalysts ammonia is decomposed to N_2 and H_2; accordingly, the concentration of unlabeled $^{14}N_2$ increases.

The order observed for the onset temperature of reduction of stored NO_x (i.e. $T(H_2) < T(NH_3)$) compares fairly well with the efficiency of the reductants in scavenging the O-adatoms from Pt(Rh)-O and then in the activation of stored NO_x by metal reduced centers, that seems to represent the rate determining step of the reduction of stored NO_x [10]. In the presence of efficient reductants like H_2 (and NH_3), it is likely that NO formed upon the activation of stored NO_x does not desorb from the metal sites, but is readily decomposed to N- and O-adatoms over them. Once formed, O-adatoms are scavenged by H-adatoms formed upon decomposition of H_2 and of NH_3 with formation of H_2O whereas N-adatoms combine to form N_2 (or are hydrogenated to give NH_3 in the case of H_2), which are indeed observed among the reaction products. Nevertheless, it is not possible to exclude that NO might be released in the gas phase and subsequently re-adsorbed and decomposed at metal sites to give N_2 and NH_3.

When the reactivity of the reductant is lower, like in the case of NH_3, oxidized metal sites are less efficiently reduced to metal form. Accordingly, released NO is not readily decomposed into N- and O-adatoms over partially O-covered metal site, so the detection of traces of N_2O is also possible. Upon increasing the temperature, the evolution of N_2O is no more observed, because ammonia efficiently scavenge O-adatoms from metal, and this favors NO decomposition to N- and O-adatoms and subsequent coupling of N-adatoms to give N_2.

Note that N_2O is observed in greater amounts only in the presence of Pt, while over Rh-monometallic catalysts its concentration is lower. This could be related to the poor reactivity of Rh with respect to Pt at low temperature. Moreover, Rh becomes active at higher temperature where ammonia is already efficient in the O-adatoms removal.

3.2.4 Reactivity of the stored species under realistic conditions

In a previous work by some of us [29], Pt- and Rh-based catalysts have been tested under lean/rich conditions at different temperatures. It has been found that the Rh-based samples exhibit a superior ability to release O_2 from the surface at lower temperatures with respect to Pt, suggesting the presence

of a promoting effect on the spillover process of NO_x to the precious metal, controlling the subsequent release and reduction of NO_x. Aiming to a better understanding of the different catalytic behavior of Rh- and Pt-based catalysts, we have here analyzed the behavior of the bimetallic Pt-Rh catalyst and monometallic references in the lean-rich cycles using a complex reducing mixture, maintaining a continuous flow of CO_2 and water.

Reactivity of NO_x Species Stored at 250°C - Figure 11A-C show the gas-phase results obtained during the lean-rich cycles performed at 250°C over Pt-Rh-Ba, Pt-Ba and Rh-Ba catalysts, respectively. Note that in the Figure is reported a representative cycle, i.e. the catalysts are fully conditioned at this temperature.

In the case of the Pt-Rh-Ba sample (Figure 11A), the breakthrough of NO was detected after 30 s. Then, the nitrogen oxide concentration increases with time, until a steady state is reached (near 800 ppm). The NO_x storage is accompanied by evolution of NO_2 (near 60 ppm) due to oxidation of NO over Pt (Rh) sites. After 15 min, at the end of the lean phase 2.66 10^{-4} mol/g_{cat} result stored onto the catalyst surface. Then, the NO concentration is decreased to zero in a stepwise manner and the reducing mixture (H_2 + CO + C_3H_6) is fed. At the lean-to-rich switch a tailing in the NO_x concentration is observed due to the desorption of weakly NO_x adsorbed (near 2.68 10^{-5} mol/g_{cat}); an instantaneous production of N_2 and of N_2O is observed, along with NH_3 which is however detected with a delay. At the rich-to lean transition a new N_2O peak is observed.

Similar behavior is observed with the Pt- and Rh-monometallic catalysts (Figure 11B and 11C, respectively). Over Pt-Ba/Al_2O_3 the NO_x breakthrough is observed after 60 s; after 15 min of lean phase NO reaches near 700 ppm while NO_2 accounts for 160 ppm, i.e. the oxidation capacity is higher than the bimetallic catalyst. In the case of Rh-Ba/Al_2O_3 catalyst, upon NO addition (Figure 11C) its concentration increases monotonically with time showing an almost nil dead time, while NO_2 is not observed being the NO/NO_2 oxidation not effective at this temperature. The total amount of stored NO_x result near 3.44 10^{-4} mol/g_{cat} over Pt-monometallic catalyst and near 1.7 10^{-4} mol/g_{cat} over Rh-monometallic one. Both the rich phases show the same dynamics described for the bimetallic system,

being the lowest N_2O production observed over Rh-monometallic catalyst. Only over Pt-monometallic sample, N_2O is observed also at the rich-to lean transition.

It is worth to note that over all the systems, H_2 and CO concentration are observed to increases later than propylene, when the concentration of nitrogen decreases. It would be notice that a complex set of reactions, involving the reductant species, takes place during the reduction:

i) steam reforming reaction of C_3H_6 with water (reaction (11)):

$$C_3H_6 + 3\ H_2O \rightarrow 3\ CO + 6\ H_2 \quad (11)$$

ii) water gas shift reaction (12):

$$CO + H_2 \rightarrow CO_2 + H_2O \quad (12)$$

iii) reverse water gas shift reaction (13):

$$CO_2 + H_2O \rightarrow CO + H_2 \quad (13)$$

The consumption of propylene could be related to the reduction of stored NO_x, but also to the occurrence of the steam reforming reaction (11). However, the H_2 concentration at steady state remain lower than the inlet value (i.e. 500 ppm) suggesting that or reaction (11) is not active or it is balanced by the occurrence of reaction (12) and/or reaction (13).

Reactivity of NO_x Species Stored at 350°C – At higher temperature, i.e. 350°C, the bimetallic catalyst shows a dead time in NO breakthrough of 110 s; the dead time is longer for Pt-catalyst and shorter for Rh-catalyst (near 170 s and 50 s, respectively). Also the NO/NO_2 oxidation follows the same trend, being higher for $Pt\text{-}Ba/Al_2O_3$, lower for $Rh\text{-}Ba/Al_2O_3$ and intermediate for the bimetallic system. At the end of the lean phase, the bimetallic Pt-Rh catalyst exhibits the best storage capacity ($6.04\ 10^{-4}$ mol/g_{cat}); lower mounts are calculated for the monometallic systems, being higher in the case of Pt ($4.59\ 10^{-4}$ mol/g_{cat} over Pt vs $2.74\ 10^{-4}$ mol/g_{cat} over Rh).

Then, upon the rich switch, the reductant mixture is admitted to the reactor. The NO_x concentration rapidly decreases and an instantaneous production of N_2 and of N_2O is observed, along with NH_3 which is however detected with a delay. The reduction of the stored NO_x is more selective to N_2 at this temperature since minor amounts of NH_3 and of N_2O are detected.

Finally, at this temperature the concentration of hydrogen at steady state results higher than the inlet value (i.e. 500 ppm) suggesting that the steam reforming and the reverse water gas shift reactions (11-13) occur to a higher extent than reaction (12). Moreover, the low CO concentration suggests that the water gas shift reaction (12) also occurs to some extent.

As already discussed and demonstrated in previous work [30], the reduction of the stored NO_x is based on a metal-catalyzed process that does not involve the thermal release of the stored NO_x as the preliminary step. Instead, the process is initiated by the reduction of the noble metal by the reductant; this leads to the release of NO from the NO_x species stored nearby the Me sites (Pt, Rh), and to the migration toward Pt of the species adsorbed far-away from the noble metal. This process is followed by decomposition of the released NO into N- and O-adatoms over the metal sites (reactions 14 and 15). NO dissociation as the initial step for NO_x reduction has been pointed out by transient TAP reactor experiments[31], and by other evidences as well [32].

$$NO + Me \rightarrow Me\text{-}NO \quad (14)$$

$$Me\text{-}NO + Me \rightarrow Me\text{-}N + Me\text{-}O \quad (15)$$

N-containing products are then formed upon reaction of adsorbed N-adatoms with undissociated NO, with other N-adatoms or with H-adatoms, leading to N_2O (reaction 16), N_2 (reaction 17) and NH_3 (reaction 18), respectively, while the role of the reducing agent is to remove the O-adspecies from the metal that is hence kept in a reduced state.

$$Me\text{-}NO + Me\text{-}N \rightarrow N_2O + 2\ Me \quad (16)$$

$$2\ Me\text{-}N \rightarrow 2\ Me + N_2 \quad (17)$$

$$Me\text{-}N + 3\ Me\text{-}H \rightarrow 4\ Me + NH_3 \quad (18)$$

Me-O species formed upon dissociation of NO (reaction 15) are scavenged by the reductant restoring Me sites, while Me-H species are formed by the H-activation on Me sites (H-atom deriving from both H_2 and C_3H_6).

At the active-site level, the selectivity of the reduction process depends on the operating conditions (temperature, gas-phase NO and H_2 concentration), i.e. on the degree of reduction of the noble metal

and on the local concentration of N-, H-adatoms: at low temperatures and at the beginning of the rich phase the noble metal is not fully reduced and this favors N_2O formation, whereas high temperatures and/or high H-atoms concentration favor NH_3 formation. Accordingly, high selectivity to N_2 formation is observed when a high concentration of N-adspecies is attained.

Inspection of the literature [33,34,35,36,37,38,39] reveals that during lean-rich operations over fully formulated LNT catalysts N_2O is formed. Indeed, N_2O evolution is observed at both lean-to-rich and rich-to-lean transitions (primary and secondary N_2O emissions). It has been suggested that primary N_2O formation (lean-to-rich transition) is formed at the regeneration front, when the reductant reaches oxidized/not fully reduced Platinum-Group-Metal (PGM) sites, which are in a close proximity to NO_x ad-species. The secondary N_2O formation (rich-to-lean transition) originates from reaction between residual surface NO_x with reductive species (like NCO, CO or NH_3) in an adsorbed state.

In the lean-rich cycles of Figure 11A-C and 12A-C, both primary and secondary N_2O peaks are detected with different concentration depending mainly on temperature and on the noble metal present in the catalysts. Primary N_2O is occurring during lean/rich cycles according to the lines previously depicted (reactions (14) – (16)). At high temperature primary N_2O formation is reduced because the metal sites are easier reduced by the reducing agent, and this enhances the NO dissociation thus favoring the coupling of N-adatoms forming N_2 (reaction (17)) and/or the hydrogenation to NH_3 (reaction (18)). Even if the lower N_2O production is observed for Rh-Ba/Al_2O_3 catalysts, it would seem that this is more the effect of the lower storage capacity (that means low reduction products in general) than of the specific metal activity.

At variance, secondary N_2O may originate from reaction of NO/O_2 with minor quantities of reductive species (like NCO, CO or NH_3) left adsorbed on the surface during the rich phase. This leads to the N_2O evolution observed during the rich-to-lean switch. As in the case of primary N_2O, also secondary N_2O formation is decreased as increasing the temperature being the metal sites more easily reduced. Moreover, in this case over Rh-containing catalysts, both bi- and mono-metallic, the secondary N_2O

results lower than over Pt-one at each temperature. This could be related to the different poisoning effect that CO have over Rh and Pt metal sites.

References

1 S.i. Matsumoto, Catalytic Reduction of Nitrogen Oxides in Automotive Exhaust Containing Excess Oxygen by NOx Storage-Reduction Catalyst, CATTECH, 4 (2000) 102-109

2 M. Koebel, M. Elsener, M. Kleemann, Urea-SCR: a promising technique to reduce NOx emissions from automotive diesel engines, Catalysis Today, 59 (2000) 335-345.

3 S. Roy, A. Baiker, NOx Storage−Reduction Catalysis: From Mechanism and Materials Properties to Storage−Reduction Performance, Chemical Reviews, 109 (2009) 4054-4091

4 N. Takahashi, H. Shinjoh, T. Iijima, T. Suzuki, K. Yamazaki, K. Yokota, H. Suzuki, N. Miyoshi, S.-i. Matsumoto, T. Tanizawa, T. Tanaka, S.-s. Tateishi, K. Kasahara, The new concept 3-way

catalyst for automotive lean-burn engine: NOx storage and reduction catalyst, Catalysis Today, 27 (1996) 63-69

5 LNT BOOK

6 T.W. Chan, E. Meloche, J. Kubsh, R. Brezny, Black Carbon Emissions in Gasoline Exhaust and a Reduction Alternative with a Gasoline Particulate Filter, Environmental Science & Technology, 48 (2014) 6027-6034

7 N. Le Phuc, X. Courtois, F. Can, S. Royer, P. Marecot, D. Duprez, NOx removal efficiency and ammonia selectivity during the NOx storage-reduction process over Pt/BaO(Fe, Mn, Ce)/Al2O3 model catalysts. Part I: Influence of Feand Mn addition, Applied Catalysis B-Environmental, 102 (2011) 353-361

8 C. Shi, Y. Ji, U.M. Graham, G. Jacobs, M. Crocker, Z. Zhang, Y. Wang, T.J. Toops, NOx storage and reduction properties of model ceria-based lean NOx trap catalysts, Applied Catalysis B-Environmental, 119-120 (2012) 183-196

9 J.-G. Kim, H.-M. Lee, M.-J. Lee, J.-H. Lee, J.-G. Kim, J.-Y. Jeon, S.-K. Jeong, S.-J. Yoo, S.-S. Kim, Effect of Co and Rh promoter on NOx storage and reduction over Pt/BaO/Al2O3 catalyst, Journal of Industrial and Engineering Chemistry, 14 (2008) 841-846.

10 L. Castoldi, L. Righini, R. Matarrese, L. Lietti, P. Forzatti, J. Catal. 328 (2015) 270

11 Lietti et al. ChemCatChem 4 (2012) 55–58

12 Morandi et al. Catalysis Today 231 (2014) 116–124

13 Castoldi et al. Applied Catalysis B 224 (2018) 249–263

14 Yi C-W, Kwak JH, Szanyi J (2007) J Phys Chem C 111:15299–15305

15 Daturi et al, Oil & Gas Science and Technology – Rev. IFP Energies nouvelles, Vol. 66 (2011), No. 5, pp. 845-853

16 39 in ANTONIA PAPER

17 40 in ANTONIA PAPER

18 ANTONIA PAPER

19 11 in BOOK ch 7

20 22 in BOOK ch 7

21 18, in L. Castoldi et al. / Journal of Catalysis 328 (2015) 270–279; Top Catal (2017) 60:250–254

22 23 in L. Castoldi et al. / Journal of Catalysis 328 (2015) 270–279; Top Catal (2017) 60:250–254

23 27 in L. Castoldi et al. / Journal of Catalysis 328 (2015) 270–279; Top Catal (2017) 60:250–254

24 Top Catal (2017) 60:250–254

25 Rh catalysts

26 Lietti e t al Ind. Eng. Chem. Res. 2012, 51, 7597−7605

27 23 in BOOK ch 7

28 24 in BOOK ch 7

29 20 in catalysts 2016

30 LNT BOOK ch 7

31 R. Burch, P.J. Millington and A.P. Walker, *Appl. Catal. B: Environ.*,1994, **4**, 65.

32 R. Burch, J.P. Breen, F.C. Meunier, *Appl. Catal. B: Environ.*, 2002, **39**, 283.

33 W.P. Partridge and J.S. Choi, *Appl. Catal. B: Environ.*, 2009, 91, 144

34 J.S. Choi, W.P. Partridge, J. Pihl, M-Y. Kim, P. Koĉi and C.S. Daw, *Catal Today*, 2002, **184**, 20.

35 J.P Breen, R. Burch, C. Fontaine-Gautrelet, C. Hardacre and C. Rioche, *Appl Catal B: Environ.* 2008, **81**, 150.

36 P. Dasari, R. Muncrief and M.P. Harold, *Top. Catal.*, 2013, **56**, 1922.

37 P. Pereda-Ayo, D. Duraiswami, J.A. Gonzàlez-Marcos and J.R. Gonzàlez-Velasco, *Chem. Eng. J.,* 2011, **169**, 58.

38 R.D. Clayton, M.P. Harold MP and V. Balakotaiah, *Am. Inst. Chem. Eng.*, 2009, **7**, 405.

39 S. Bàrtovà S, P. Koĉi, D. Mràĉek, M. Marek, J.A. Pihl, J-S. Choi, T.J. Toops and W.P Partridge, *Catal. Today*, 2014, **231**, 145.

Table 1 – Chemical composition and morphological and textural features of a. p. catalysts

Catalysts	Metal content (wt %)	Ba content (wt %)	SS ($m^2\ g^{-1}$)	V_P ($cm^3\ g^{-1}$)	r_P (Å)
Pt-Ba/Al_2O_3	1	16	140.2	0.72	102.3
Rh-Ba/Al_2O_3	0.5	16	149.8	0.76	102.0
Pt-Rh-Ba/Al_2O_3	Pt 1 – Rh 0.5	16	139.4	0.74	106.8

Table 2 - XPS

Catalysts	surface atomic ratio		
	Pt/Al	Rh/Al	Ba/Al
Pt-Ba/Al_2O_3	0,0019	na	0,023
Rh-Ba/Al_2O_3	na	0,0067	0,024
Pt-Rh-Ba/Al_2O_3	0,0012	0,0065	0,024

Captions to the Figures

Figure 1 - XRD pattern of Pt-Rh-Ba/Al_2O_3 (a), Rh-Ba/Al_2O_3 (b) and Pt-Ba/Al_2O_3 (c) catalysts. The reference peaks are also reported: γ-Al_2O_3 face-centered cubic (JCPDS 10-425) $BaCO_3$ witherite (JCPDS 5-378), $BaCO_3$ monoclinic (JCPDS 78-2057) and Pt face-centered cubic (JCPDS 4-802) identified by **γ**, **ε**, **ϖ** and **δ** respectively.

Figure 2 – HRTEM images of Pt-Rh-Ba/Al_2O_3 catalyst. A)-C) STEM-HAADF image; D) HRTEM images.

Figure 3 – HRTEM images of Pt-Ba/Al_2O_3 catalyst. A) STEM-HAADF image; B) enlargement of A; C) EDX spectra recorded in the areas labeled “a” and “b”; D) and E) HRTEM images.

Figure 4 – HRTEM images of Rh-Ba/Al_2O_3 catalyst. A)-E) STEM-HAADF image; F) HRTEM images.

Figure 5 – FT-IR spectra recorded during the lean phase at different temperature over Pt-Rh-Ba/Al_2O_3 catalyst. A) 150°C; B) 250°C; C) 350°C.

Figure 6 – FT-IR spectra recorded during the lean phase at different temperature over Rh-Ba/Al_2O_3 catalyst. A) 150°C; B) 250°C; C) 350°C.

Figure 7 – Thermal stability of NO_x species stored at 150°C (A,B,C), at 250°C (D,E,F) and at 350°C (G,H,L) over Pt-Rh-Ba/Al_2O_3 (A,D,G), Pt-Ba/Al_2O_3 catalyst (B,E,H) and Rh-Ba/Al_2O_3 catalyst (C,F,L) catalysts.

Figure 8 – ^{15}NO Temperature Programmed Isotopic Exchange (^{15}NO-TPIE) experiments after adsorption of nitrites (A-C) and nitrates (D-F) over Pt-Rh-Ba/Al_2O_3 (A,D), Pt-Ba/Al_2O_3 catalyst (B,E) and Rh-Ba/Al_2O_3 catalyst (C,F) catalysts. Storage conditions: NO (1000 ppm) + O_2 (3% v/v) in He at 150°C (nitrites) or 350°C (nitrates).

Figure 8 – Temperature Programmed Surface Reaction (TPSR) of nitrates with H_2 (A-C) and NH_3 (D-E) over Pt-Rh-Ba/Al_2O_3 (A,D), Pt-Ba/Al_2O_3 catalyst (B,E) and Rh-Ba/Al_2O_3 catalyst (C,F) catalysts. Storage conditions: NO (1000 ppm) + O_2 (3% v/v) in He at 350°C (nitrates).

Figure 10 – Temperature Programmed Surface Reaction (TPSR) of nitrites with H_2 (A-C) and NH_3 (D-E) over Pt-Rh-Ba/Al_2O_3 (A,D), Pt-Ba/Al_2O_3 catalyst (B,E) and Rh-Ba/Al_2O_3 catalyst (C,F) catalysts. Storage conditions: NO (1000 ppm) + O_2 (3% v/v) in He at 150°C (nitrites).

Figure 12 – Isothermal lean-rich cycles at 250°C (A,B,C) and 350°C (D,E,F) over Pt-Rh-Ba/Al_2O_3 (A,D), Pt-Ba/Al_2O_3 catalyst (B,E) and Rh-Ba/Al_2O_3 catalyst (C,F) catalysts. Lean conditions: NO (1000 ppm) + O_2 (3% v/v) in He + CO_2 (975 ppm) + H_2O (2.5%); rich conditions: H_2 (500 ppm) + CO (1500 ppm) + C_3H_6 (450 ppm) in He + CO_2 (975 ppm) + H_2O (2.5%).

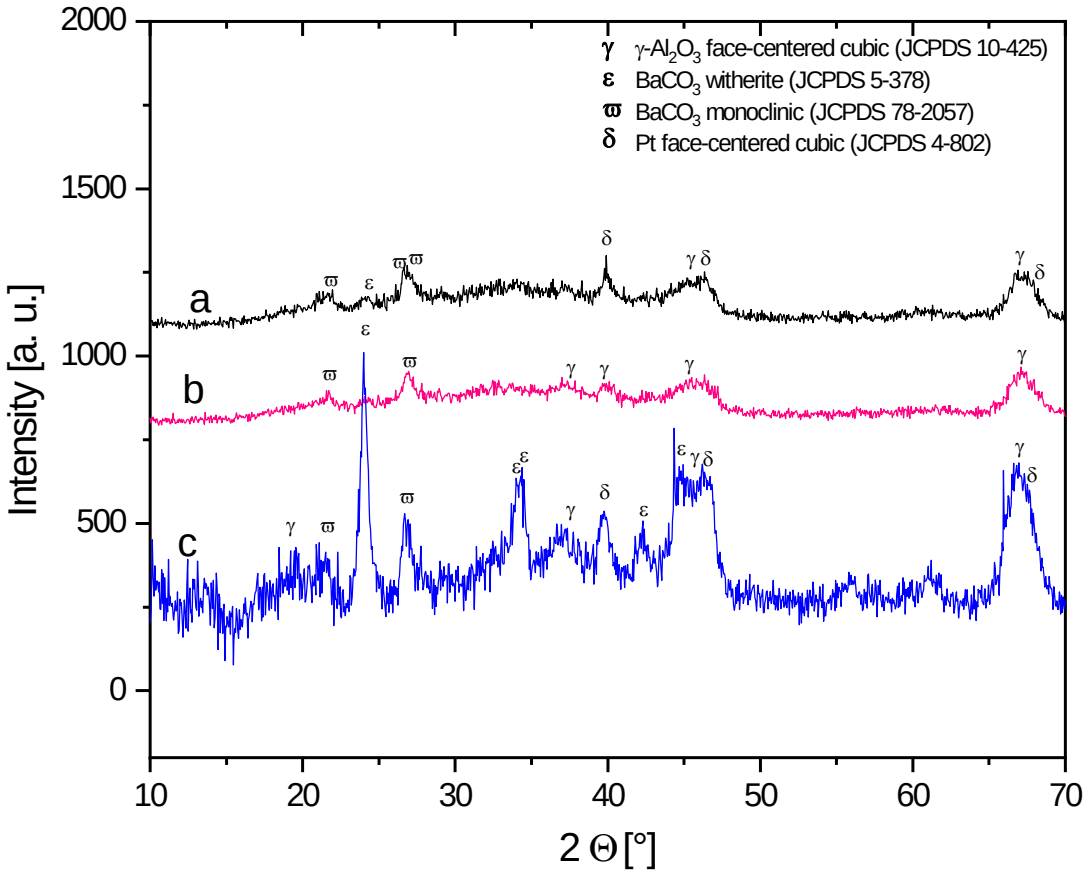
γ γ-Al2O3 face-centered cubic (JCPDS 10-425)
ε BaCO3 witherite (JCPDS 5-378)
ϖ BaCO3 monoclinic (JCPDS 78-2057)
δ Pt face-centered cubic (JCPDS 4-802)
Intensity [a. u.]
2 Θ [°]
a
b
c
0
500
1000
1500
2000
10
20
30
40
50
60
70

Figure 1

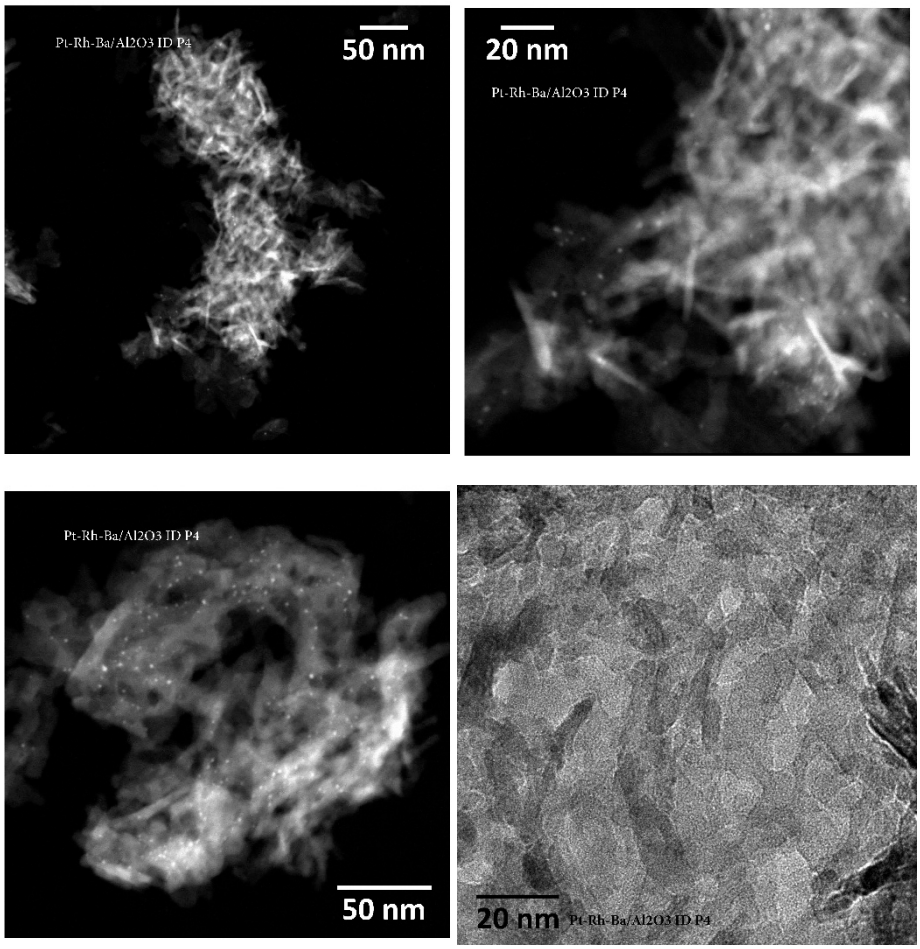
Pt-Rh-Ba/Al2O3 ID P4
50 nm
20 nm
Pt-Rh-Ba/Al2O3 ID P4
Pt-Rh-Ba/Al2O3 ID P4
50 nm
20 nm
Pt-Rh-Ba/Al2O3 ID P4

Figure 2

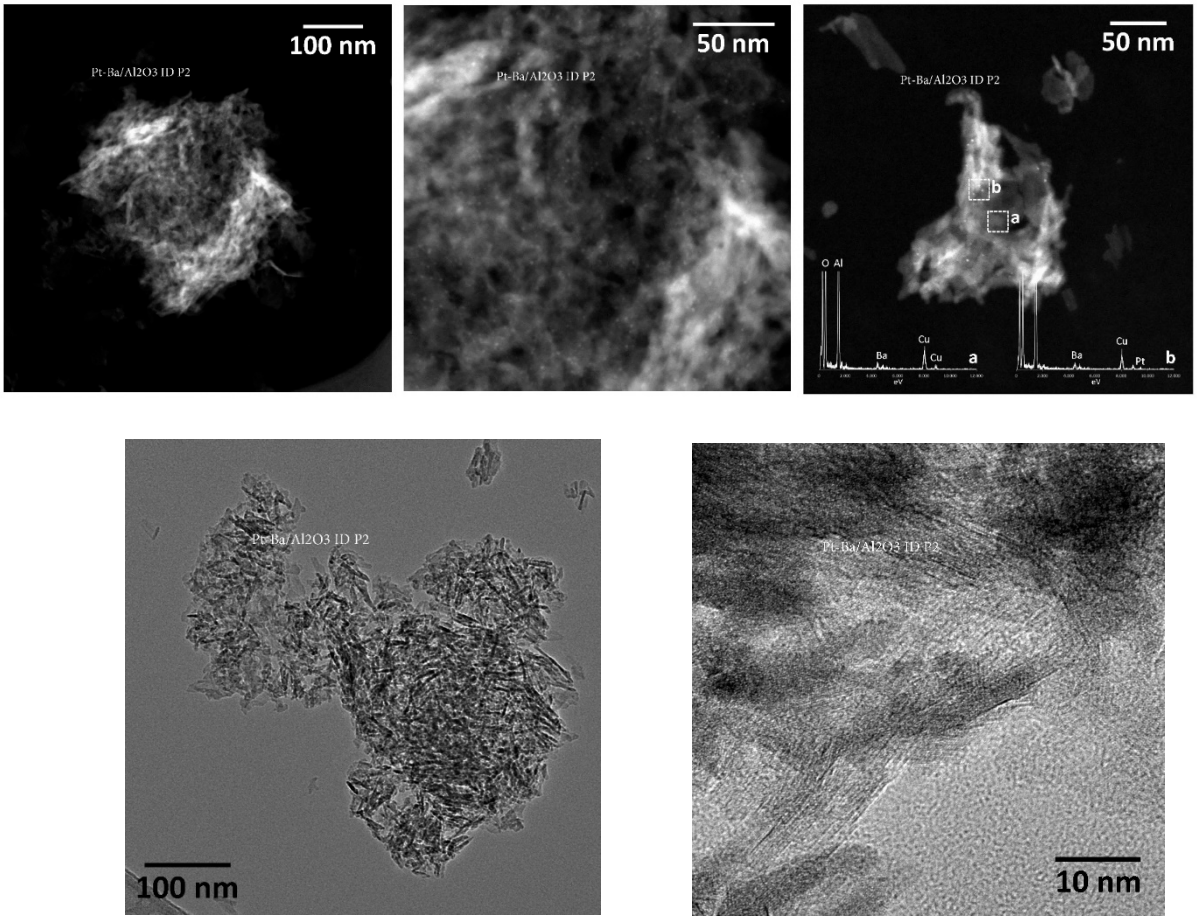
100 nm
Pt-Ba/Al2O3 1D P2
50 nm
Pt-Ba/Al2O3 1D P2
50 nm
Pt-Ba/Al2O3 1D P2
b
a
O Al
Ba
Cu
Cu
a
Ba
Cu
Pt
b
Pt-Ba/Al2O3 1D P2
100 nm
Pt-Ba/Al2O3 1D P2
10 nm

Figure 3

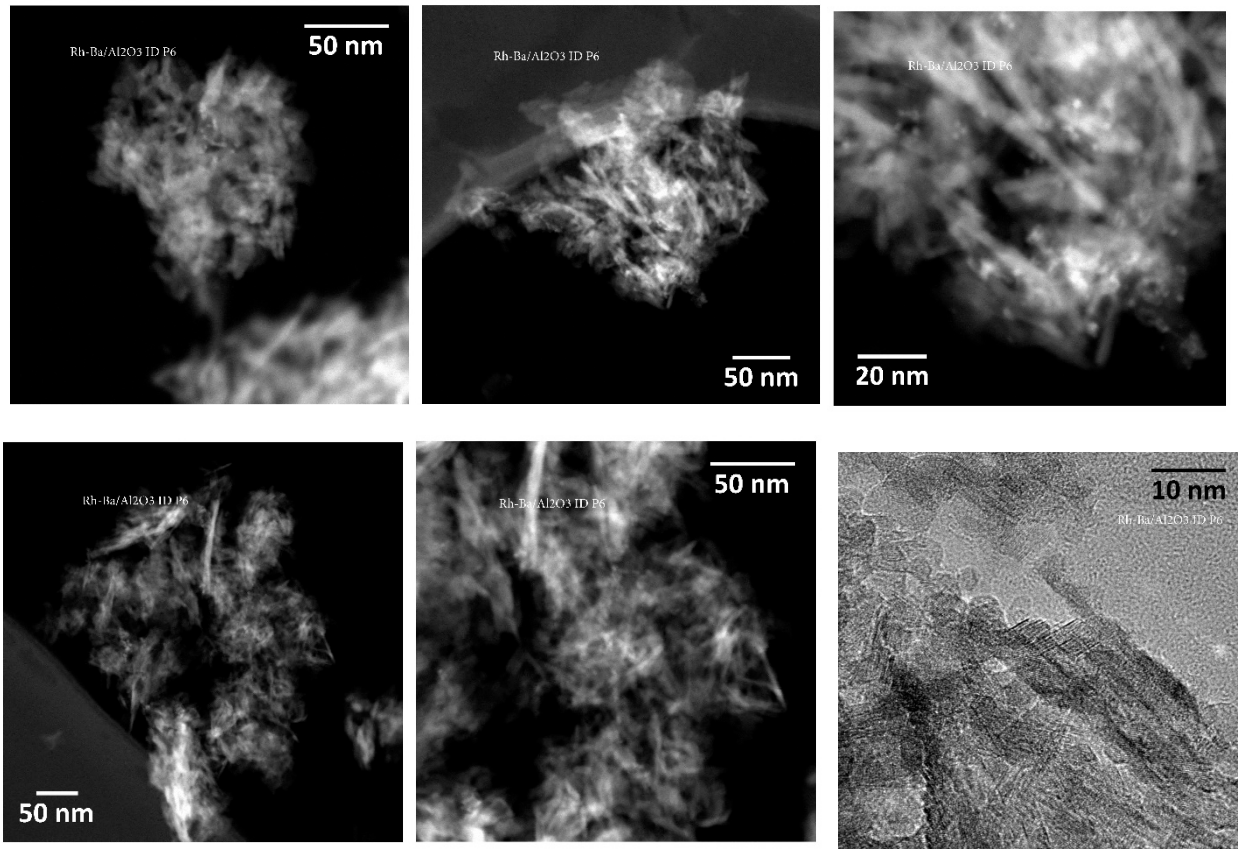
Rh-Ba/Al2O3 ID P6
50 nm
Rh-Ba/Al2O3 ID P6
50 nm
Rh-Ba/Al2O3 ID P6
20 nm
Rh-Ba/Al2O3 ID P6
50 nm
Rh-Ba/Al2O3 ID P6
50 nm
10 nm
Rh-Ba/Al2O3 ID P6

Figure 4

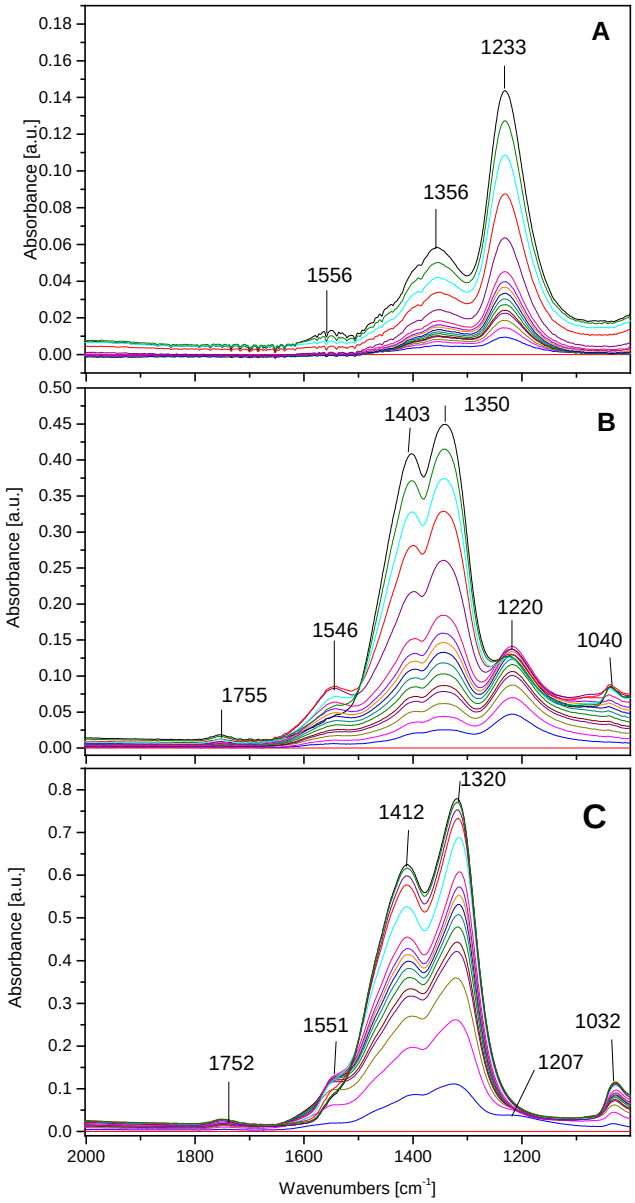
A
1233
1356
1556
Absorbance [a.u.]
B
1403
1350
1220
1546
1040
1755
C
1320
1412
1551
1032
1752
1207
2000
1800
1600
1400
1200
Wavenumbers [cm-1]

Figure 5

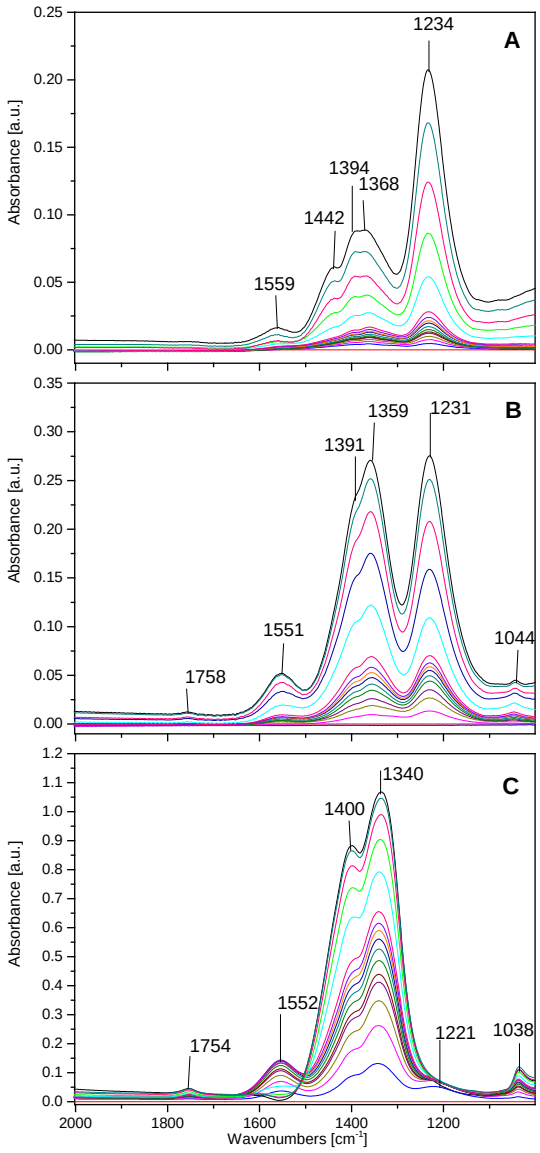
A
1234
1394
1368
1442
1559
B
1359
1231
1391
1551
1044
1758
C
1340
1400
1552
1221
1038
1754
Absorbance [a.u.]
Wavenumbers [cm-1]

Figure 6

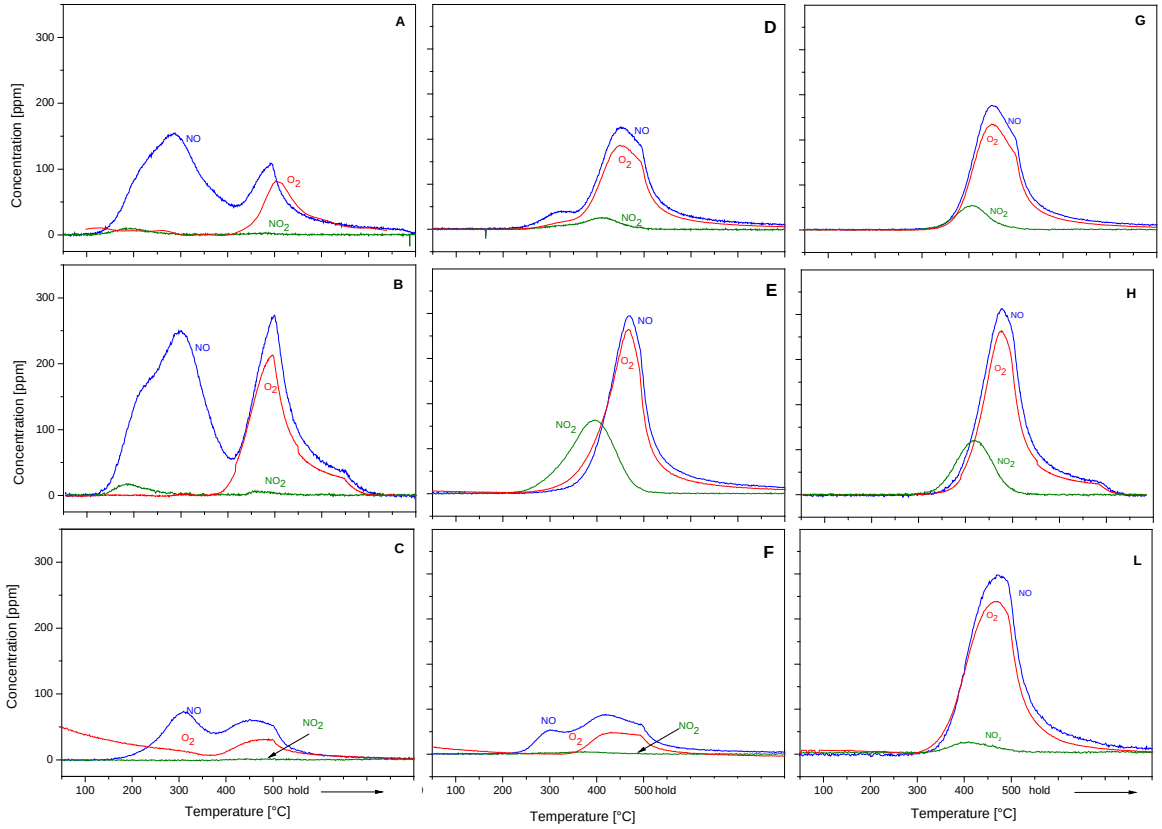
A
B
C
D
E
F
G
H
L
NO
O2
NO2
Concentration [ppm]
0
100
200
300
100
200
300
400
500 hold
Temperature [°C]

Figure 7

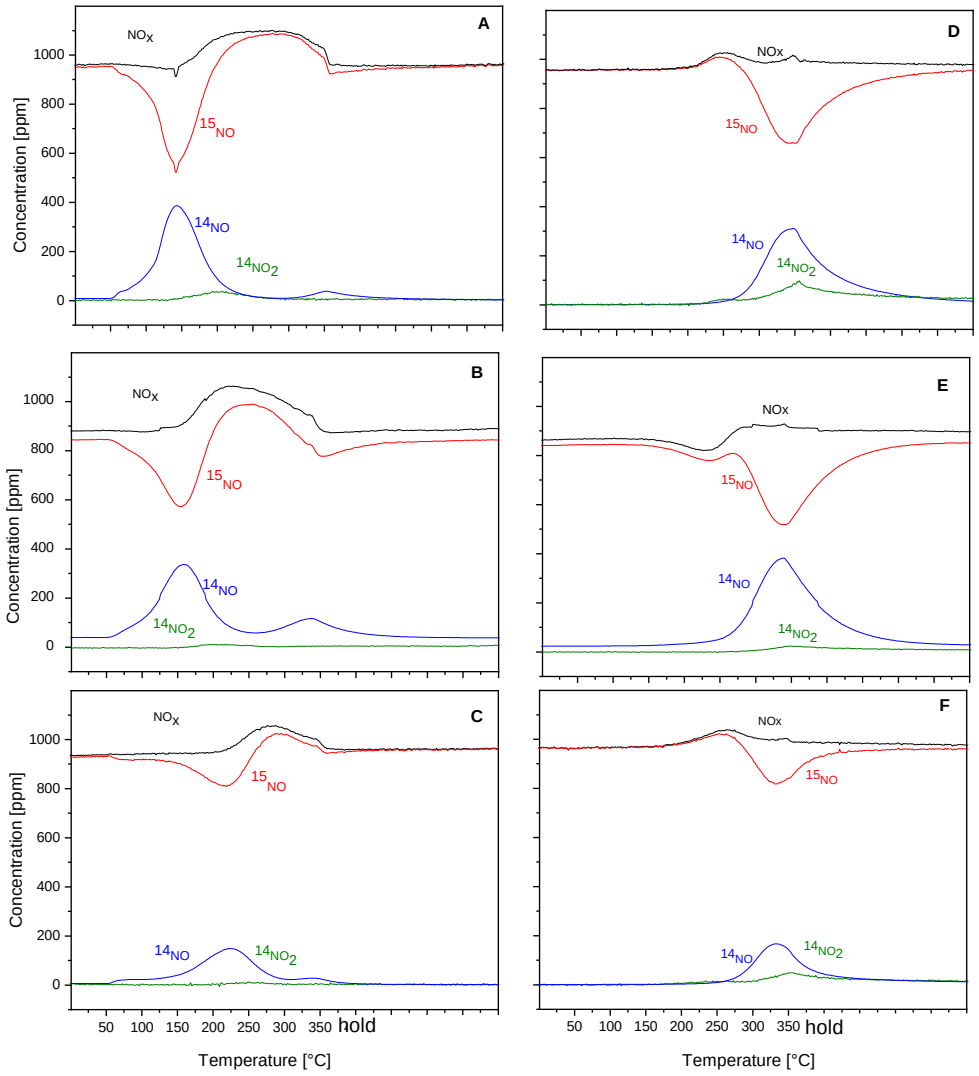
A
B
C
D
E
F
NOx
15NO
14NO
14NO2
Concentration [ppm]
0
200
400
600
800
1000
50
100
150
200
250
300
350
hold
Temperature [°C]

Figure 8

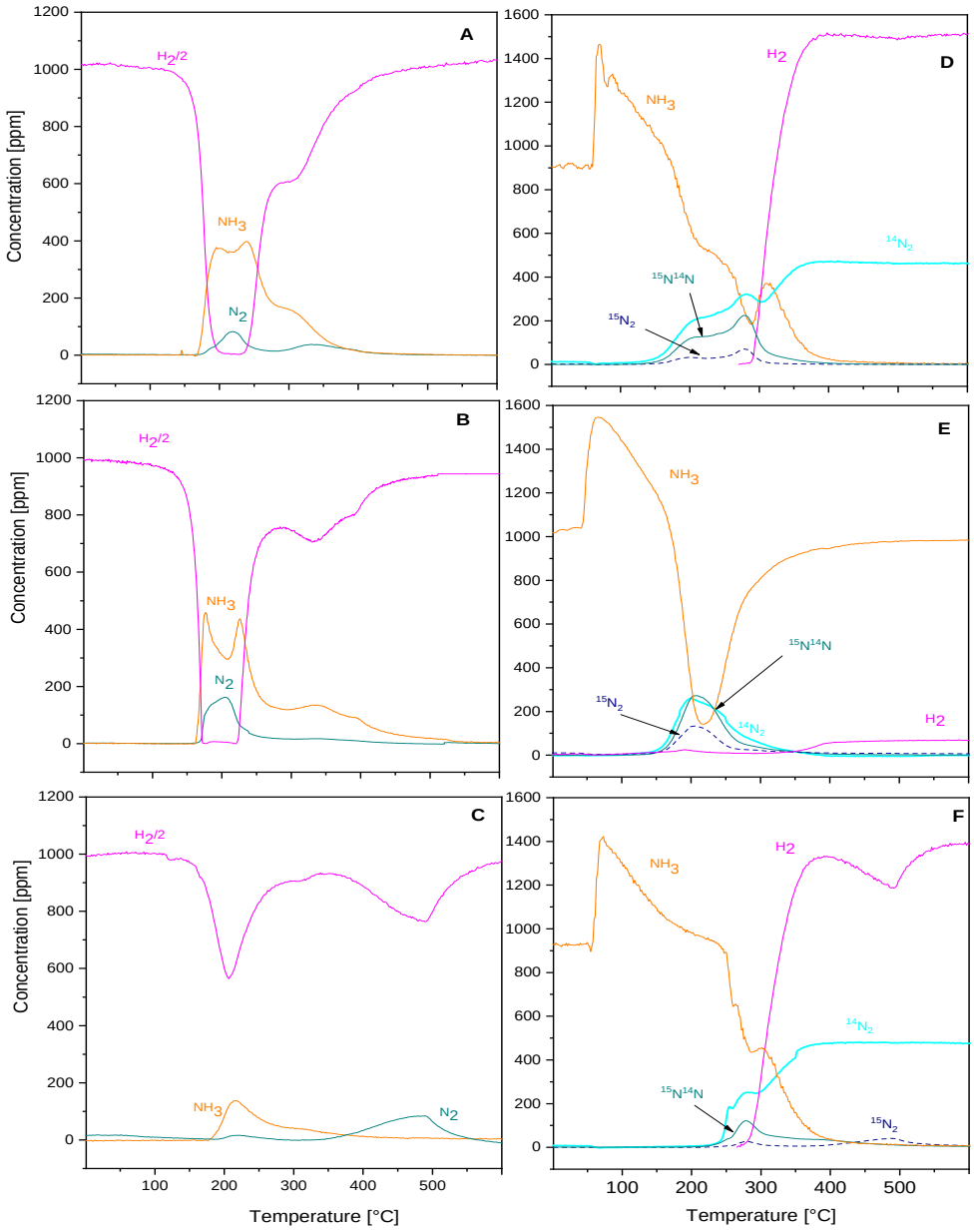
A
B
C
D
E
F
Concentration [ppm]
Temperature [°C]
H2/2
NH3
N2
H2
14N2
15N14N
15N2

Figure 9

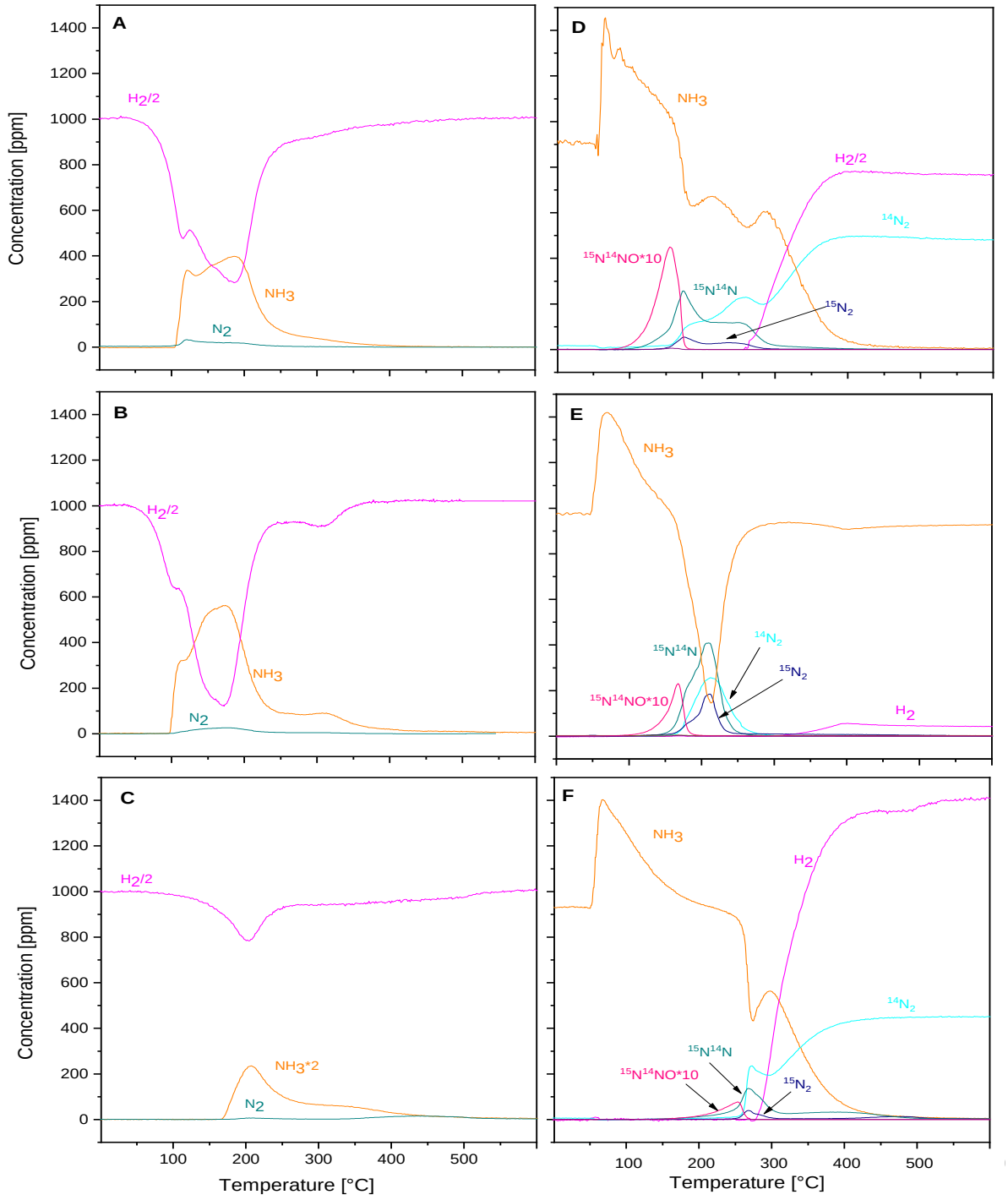
A
B
C
D
E
F
Concentration [ppm]
Temperature [°C]
H2/2
NH3
N2
NH3*2
15N14NO*10
15N14N
14N2
15N2
H2

Figure 10

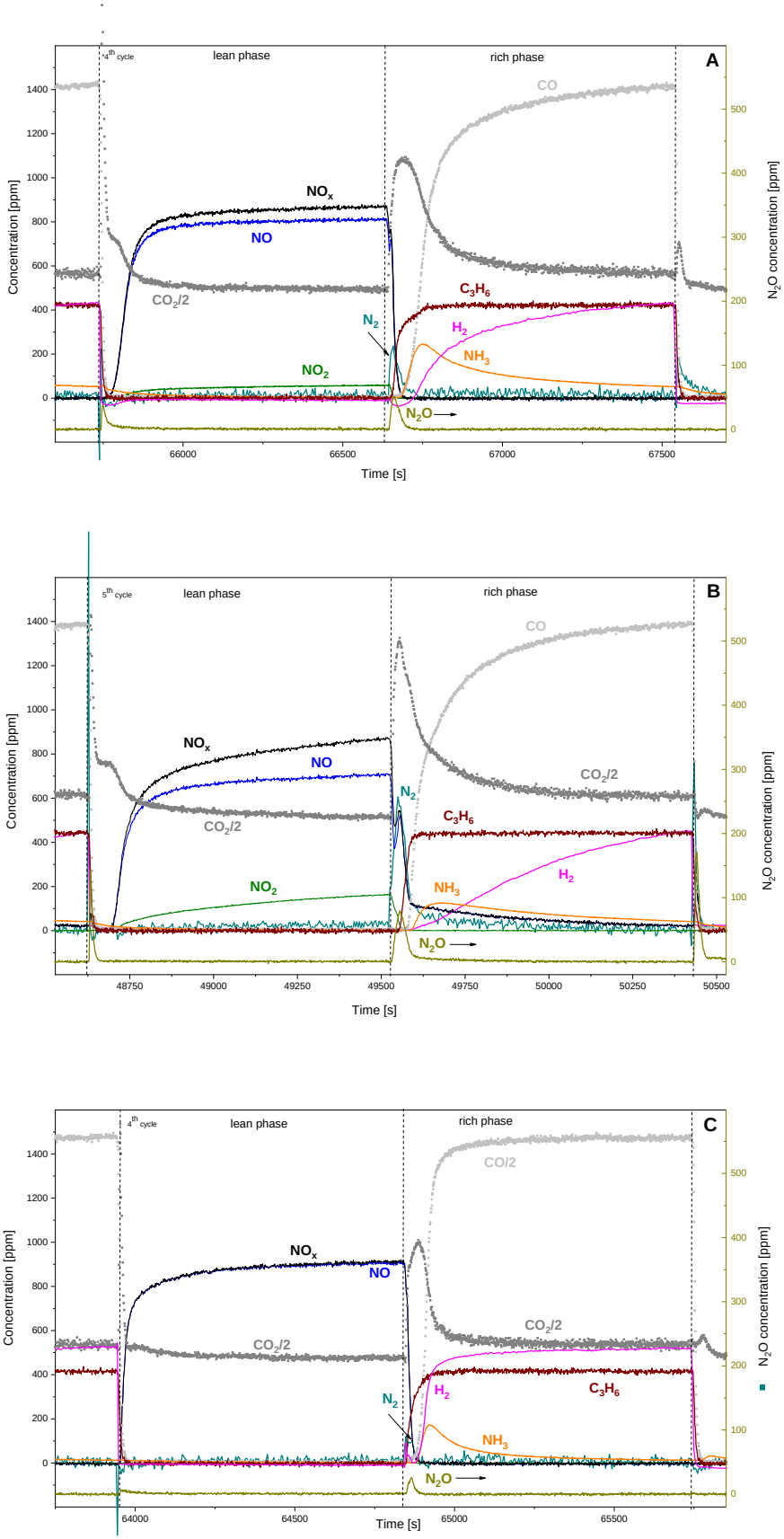
A
4th cycle
lean phase
rich phase
CO
NOx
NO
CO2/2
C3H6
N2
H2
NH3
NO2
N2O
Concentration [ppm]
N2O concentration [ppm]
Time [s]
B
5th cycle
lean phase
rich phase
CO
NOx
NO
CO2/2
N2
C3H6
H2
NH3
NO2
N2O
Concentration [ppm]
N2O concentration [ppm]
Time [s]
C
4th cycle
lean phase
rich phase
CO/2
NOx
NO
CO2/2
CO2/2
H2
C3H6
N2
NH3
N2O
Concentration [ppm]
N2O concentration [ppm]
Time [s]

Figure 11

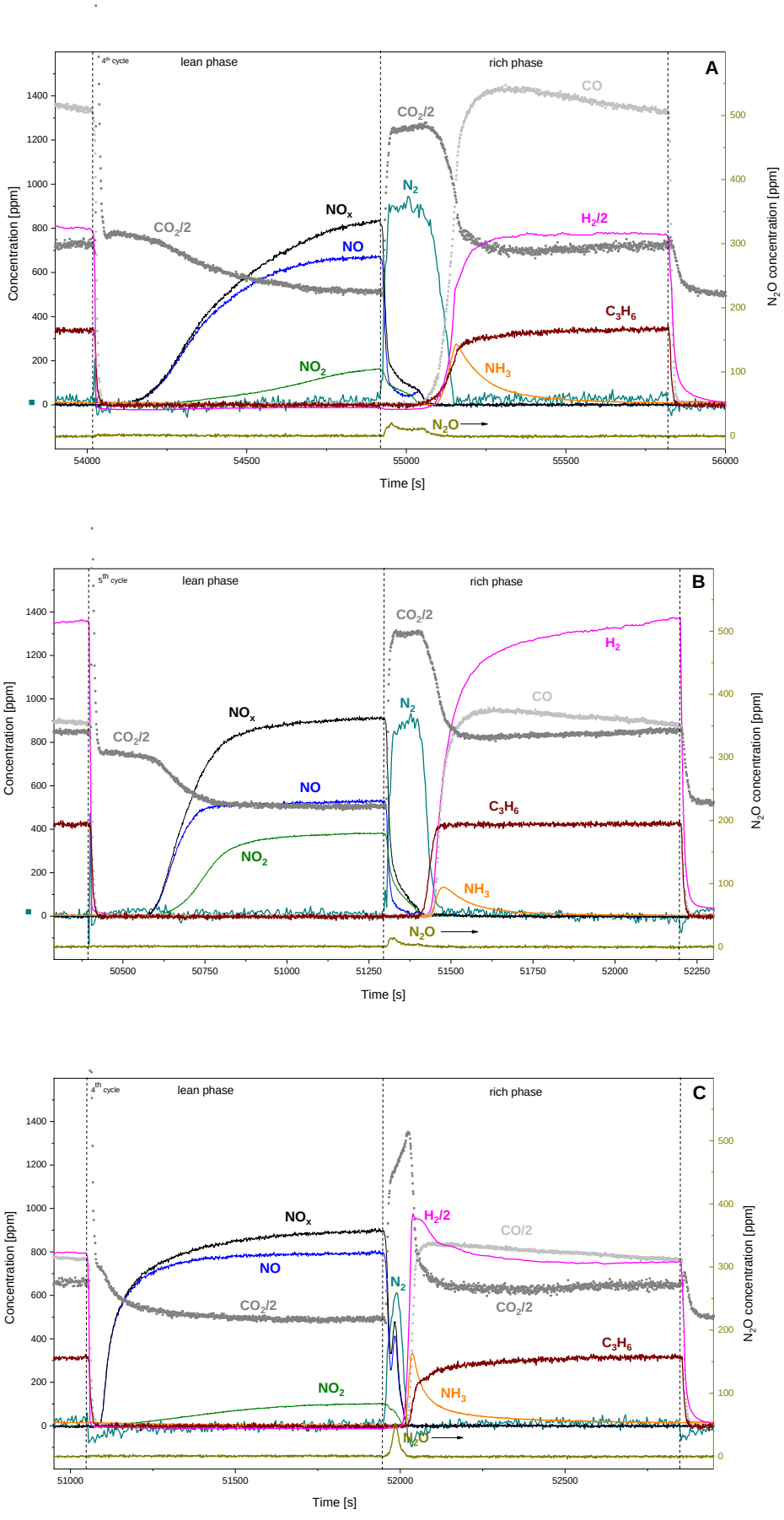
A
4th cycle
lean phase
rich phase
CO
CO2/2
N2
NOx
H2/2
CO2/2
NO
C3H6
NO2
NH3
N2O
Concentration [ppm]
N2O concentration [ppm]
Time [s]
B
5th cycle
lean phase
rich phase
CO2/2
H2
N2
NOx
CO
CO2/2
NO
C3H6
NO2
NH3
N2O
Concentration [ppm]
N2O concentration [ppm]
Time [s]
C
4th cycle
lean phase
rich phase
NOx
H2/2
CO/2
NO
N2
CO2/2
CO2/2
C3H6
NO2
NH3
N2O
Concentration [ppm]
N2O concentration [ppm]
Time [s]

Figure 12